

# Strange Attractors of Memristor and Devil's Staircase Route to Chaos

Sadataka Furui and Tomoyuki Takano

Graduate School of Teikyo University

1-1 Toyosatodai, Utsunomiya, 320-8551 Japan \*

October 24, 2018

## Abstract

We made the chaotic memristic circuit proposed by Chua and analyzed the behavior of the voltage of the capacitor, electric current in the inductor and the voltage of the memristor by adding an external sinusoidal oscillation, and studied Devil's staircase route to chaos.

When the driving oscillation  $\gamma \sin \omega t$  is increased, we observed a wide window of single node and narrower windows of oscillation. We compared the frequency of the driving oscillation  $f_s$  and the frequency of the response  $f_d$  in the window and assigned  $W = f_s/f_d$  to each window. When capacitor  $C = 1.2$ , we observed Farey sequences of  $W = \{\frac{1}{2}, \frac{2}{3}, \frac{3}{4}, \frac{4}{5}, \dots, \frac{8}{9}, \frac{1}{1}\}$ , which is expressed as  $\frac{q+Q}{p+P}$  with  $p = 2, q = 1, P = 1, Q = 1$  which converges  $Q/P = 1/1$  and  $W = \{\frac{9}{11}, \frac{11}{13}, \frac{13}{15}, \frac{15}{17}, \frac{2}{2}\}$  with  $Q/P = 2/2$ . It has other Farey sum sequences  $W = \{\frac{3}{5}, \frac{4}{7}, \dots, \frac{1}{2}\}$  and  $W = \{\frac{5}{8}, \frac{7}{9}, \dots, \frac{2}{1}\}$ . When  $C = 1$ , we observe only the sequence that converges to  $1/1$ .

Possible role of octonions in the sequence is discussed.

---

\*E-mail address: furui@umb.teikyo-u.ac.jp

# 1 Introduction

In 1993, Hayes, Grebogi and Ott[1] discussed an electronic circuit in a chaotic regime, using the characterization of chaos as deterministic noise[2]. Typical evolution equation of the physical system is characterized by

$$\dot{\mathbf{x}}(t) = \mathbf{F}_\mu(\mathbf{x}(t))$$

where  $\mathbf{x}$  is a set of coordinates in  $R^m$  and  $F_\mu(\mathbf{x})$  determines the nonlinear time evolution. The nature of asymptotic motion depends upon the parameter  $\mu$  and the change of the asymptotic motion is called bifurcation. Chaos is characterized by sensitivity to the initial condition, or the dependence on the difference of orbits

$$d(t) = |\mathbf{s}'(t) - \mathbf{s}(t)| \sim e^{\lambda_1 t}.$$

The parameter  $\lambda_1$  is called the largest Lyapunov coefficient.

How to measure the strangeness and the dimension of attractors was discussed by Grassberger and Procaccia[3]. In 1984, Grebogi et al.[4] showed that there are strange attractors whose Lyapunov exponents are negative. They showed that some chaotic attractors becomes nonstrange by certain weak perturbations, and the structure of Strange Nonchaotic Attractor (SNA) is rather complicated.

When a compact set  $S$  is covered by  $N(r)$  cubes of edge length  $r$ , and each cube  $i$  is associated with the probability  $p_i(r)$ , we define the capacity dimension  $D_0$  as

$$D_0 = \lim_{r \rightarrow 0} \frac{N(r)}{|\log r|},$$

and the information dimension  $D_1$  as

$$D_1 = \lim_{r \rightarrow 0} \frac{H(r)}{\log r}$$

where

$$H(r) = \sum_{i=1}^{N(r)} p_i(r) \log p_i(r)$$

Ding, Grebogi and Ott[5] studied a differential equation of a pendulum

$$\frac{d^2\phi(t)}{dt^2} + \nu \frac{d\phi(t)}{dt} + g \sin \phi(t) = F + G \sin(\omega_1 t + \alpha_1) + H \sin(\omega_2 t + \alpha_2),$$

where  $\omega_1$  and  $\omega_2$  are incommensurate, and defined  $\omega_1/\omega_2 = \omega$ . They considered a discrete map

$$\phi_{n+1} = F(\phi_n, \theta_n) \tag{1}$$

$$\theta_{n+1} = [\theta_n + 2\pi\omega] \tag{2}$$

where a square bracket indicates modulo  $2\pi$ , and conjectured that  $D_0 = 2$  and  $D_1 = 1$ . The structure of the attractor of dynamical systems defined by two variables  $(x, \theta)$  and whose Lyapunov exponents are non positive is studied by [6, 7, 8] and [9]. The conjecture on  $D_0$  and  $D_1$  were confirmed in [10]. Parameters that distinguish fractal torus configurations and chaotic configurations are important.

In 1971, Chua [11] proposed that in addition to resistor, inductor and conductor, there is an interesting non-linear circuit element which is called memristor, a combination of memory and resistor. Chua and Kang [12] represented the dynamical system, which is called memristive system by

$$\begin{aligned} \dot{x} &= f(x, u, t) \\ y &= g(x, u, t)u \end{aligned} \tag{3}$$

where  $u$  and  $y$  denote the input and the output of the system and  $x$  denotes the state of the system. Muthuswamy and Chua[13] showed that one can produce a non linear memristor and combined with inductor, capacitor and opeamp, one can observe chaotic behaviors. The chaotic behavior of memristic system was analyzed in [14, 15, 16] and [17].

Chaos in electronic circuits that consists of capacitors, inductors, resistors and opeamp was studied in 1986 by Chua, Komuro and Matsumoto[18]. When an external current source is added to the Chua's circuit, a Farey sequence period adding law was observed by Pivka,

Zhelenyak and Chua[20]. Analyses of driven Chua's circuit were done in [23, 24] and in [25]. We analyzed the chaotic behaviors of Chua's circuit by adding an external current in the system[26]. In this paper, we add an external oscillation of current to the memristic system, which we call Muthuswamy-Chua's circuit (MC circuit) and study changes in the chaotic behaviors due to an addition of driving currents.

Electrons are described by spinors and in the spinor theory of Cartan[28], self-dual vector field  $X_i (i = 1, 2, 3, 4)$  is produced from spinors as a Plücker coordinate. Spinors are described by quaternions  $\mathcal{H}$  and bispinors that consists of two quaternions with a new imaginary unit  $l$  composes an octonion,

$$\mathcal{O} = \mathcal{H} + l\mathcal{H}$$

which has the automorphism  $G_2$  group. There are 24 dimensional bases in the  $G_2$  group, and it has the triality symmetry. We study the electro magnetic field of the memristor using the octonion bases[29, 30].

The paper is organized as follows. In Sect.2, we present chaos in Chua's circuit, and in Sect.3 we present Chaos in Memristic circuit. In Sect.4, Strange nonchaotic attractor in driven memristor is studied, and in Sect.5, the resonance frequency of the driven MC circuit is analyzed by using octonion basis. Difference of strange chaotic attractors and strange nonchaotic attractor (SNA) are discussed in Sect.6.

## 2 Chaos in Chua's circuit

Chua's circuit consists of an autonomous circuit which contains a three-segments piecewise-linear resistor, two capacitors, one inductor and a variable resistor [18]. The equation of the circuit is described by the coupled differential equation

$$\begin{cases} C_1 \frac{d}{dt} v_{C1} = G(v_{C2} - v_{C1}) - \tilde{g}(v_{C1}, m_0, m_1) \\ C_2 \frac{d}{dt} v_{C2} = G(v_{C1} - v_{C2}) + i_L \\ L \frac{d}{dt} i_L = -v_{C2} \end{cases} \quad (4)$$

The three-segment piecewise-linear resistor which constitutes the non-linear element is characterized by

$$\tilde{g}(v_{C1}, m_0, m_1) = (m_1 - m_0)(|v_{C1} + B_p| - |v_{C1} - B_p|)/2 + m_0 v_{C1},$$

where  $B_p$  is chosen to be 1V,  $m_0$  is the slope (mA/V) outside  $|v_{C1}| > B_p$  and  $m_1$  is the slope inside  $-B_p < v_{C1} < B_p$ .

Here  $v_{C1}$  and  $v_{C2}$  are the voltages of the two capacitors (in V),  $i_L$  is the current that flows in the inductor (in A),  $C_1$  and  $C_2$  are capacitance (in F),  $L$  is inductance (in H), and  $G$  is the conductance of the variable resistor (in  $\Omega^{-1}$ ).

The function  $\tilde{g}(v_{C1}, m_0, m_1)$  can be regarded as an active resistor. If it is locally passive the circuit is tame, but when it is locally active it keeps supplying power to the external circuit. The chaotic behavior is expected to be due to the power dissipated in the passive element. A difference from the van der Pol circuit is that the passive area and the active area are not separated by the strange attractor, but they are entangled. The orbit in the  $v_{C1} - v_{C2}$  plane shows a double scroll orbit or a hetero-clinic orbit (i.e. an orbit which starts from a fixed point to another fixed point). We assign  $v_{C1}$ ,  $v_{C2}$  and  $i_L$ , with a specific normalization,  $x$ ,  $y$  and  $z$ , respectively.

We did not control chaotic circuits by triggering simple electronic pulse as [19], when the orbit arrives in a certain region which we assigned 'e' from which complication of the orbit starts. Main difference from [19] was that we have chosen a proper height of the pulse, so that the periodic trajectory was kept and we did not need to reset the current.

$$\begin{cases} \dot{x} = \alpha(y - h(x)) \\ \dot{y} = x - y + z \\ \dot{z} = -\beta y \end{cases}$$

where

$$h(x) = m_1 x + \frac{1}{2}(m_0 - m_1)[|x + 1| - |x - 1|]$$

$$h(x) = \begin{cases} m_1x + (m_0 - m_1) & x \geq 1 \\ m_0x & |x| \leq 1 \\ m_1x - (m_0 - m_1) & x \leq -1 \end{cases}$$

is a piecewise linear equation.

We observed that periodic double scroll is running on heteroclinic orbits. A periodic double scroll can be moved to a homoclinic orbit (i.e. an orbit which has single fixed point) by triggering a pulse when the orbit arrives at a certain region. A simulation of the Chua's circuit was done in [23]. Sinusoidally driven Chua's circuit was shown to have the Arnold's tongue and devil's staircase structure in the dynamical structure of the voltage[20], and the sinusoidally-driven double scroll Chua circuit was analyzed by Baptista and Caldas[24].

Bifurcation and routes to chaos in other sinusoidally-driven extended Chua circuits was discussed by Thamilmaran and Lakshmanan[25].

### 3 Chaos in Muthuswamy-Chua's circuits

In the study of chaotic behaviors in electronic circuits, Chua's electronic devices have attracted constant research interests.

In 2010, Muthuswamy and Chua[13] showed that a system with an inductor, capacitor and non-linear memristor can produce a chaotic circuit. The three-element circuit with the voltage across the capacitor  $x(t) = v_C(t)$ , the current through the inductor  $y(t) = i_L(t)$  and the internal state of the memristor  $z(t)$  satisfy the equation

$$\begin{cases} \dot{x} = \frac{y}{C} \\ \dot{y} = \frac{-1}{L}[x + \beta(z^2 - 1)y] \\ \dot{z} = -y - \alpha z + yz. \end{cases} \quad (5)$$

We produced the similar circuit element as Muthuswamy and Chua, measured the circuit

through the inductor, and the voltage across the capacitor. We choose

$$\begin{aligned} C &= I_s C_n T_s \\ L &= \frac{L_n T_s}{I_s} \\ \beta &= \frac{\beta_{5kpot}}{R} \\ \alpha &= \frac{1}{T_s C_f \alpha_{10kpot}} \end{aligned} \quad (6)$$

where  $I_s = 10000$ ,  $C_n = 1\text{nF}$ ,  $T_s = 10^5$ ,  $L_n = 360\text{mH}$ ,  $R = 1\text{k}\Omega$ ,  $C_f = 10\text{nF}$ .

The chaotic attractor  $i_L(t) = y$  versus  $v_C(t) = x$  obtained by experiment, and by simulation are shown in Fig.1 and 2, respectively. Here we took  $\beta = 1.43$

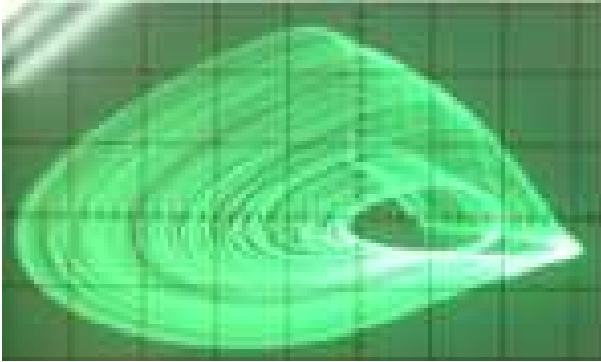


Figure 1: The chaotic attractor  $i_L(t)$  versus  $v_C(t)$ . Experimental result.

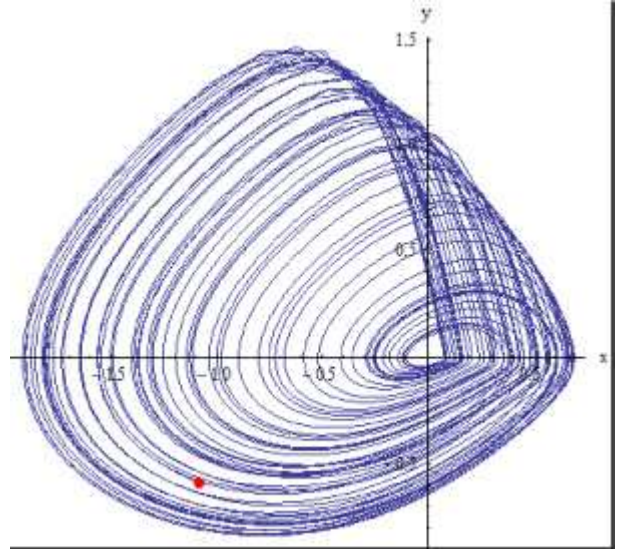


Figure 2: The chaotic attractor  $i_L(t)$  versus  $v_C(t)$ . Numerical simulation.

When  $\dot{z} = 0$ , the eq. (5) becomes  $-\alpha z + (z - 1)y = 0$  and  $z = \frac{y}{y - \alpha}$ .

Muthuswamy and Chua defined memristor equation by replacing  $y$  by  $i_M$  and  $v_L + v_c = v_M$  as

$$\begin{aligned} v_M(t) &= \beta(z^2 - 1)i_M(t) \\ \dot{z} &= i_M(t) - \alpha z - i_M(t)z \end{aligned} \quad (7)$$

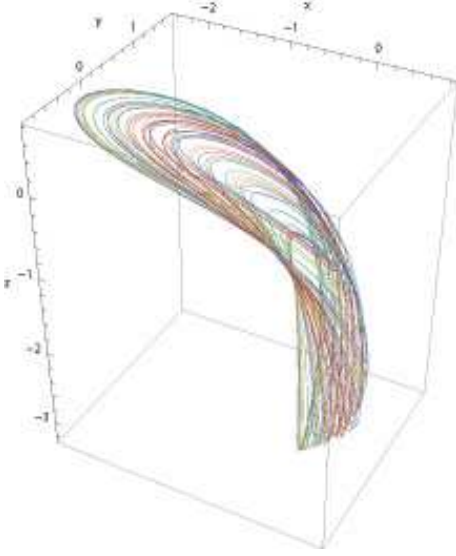


Figure 3: The attractor in the xyz-space of  $C=1, L=3.3, \alpha = 0.2, \beta = 0.5$ . Numerical simulation.

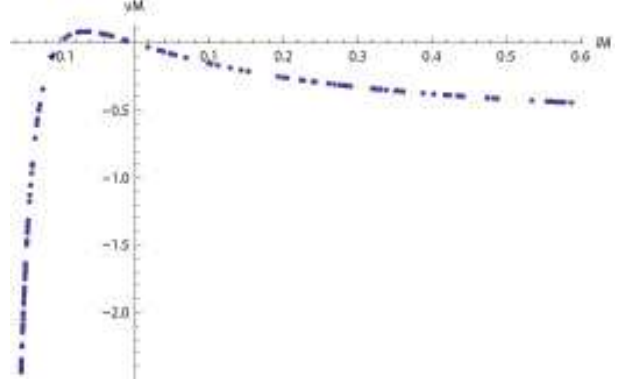


Figure 4: The DC  $v_M - i_M$  plot at  $C = 1, L = 3.3, \alpha = 0.2$ .

and by choosing  $\dot{z} = 0$ , the DC characteristic becomes

$$v_M(t) = \beta \left( \frac{i_M(t)^2}{(i_M(t) + \alpha)^2} - 1 \right) i_M(t) \quad (8)$$

When  $C=1, L=3.3$  and  $\alpha = 0.2$ , and the DC characteristic is chosen, solution of the eq.(8) which yields Lorenz like attractor becomes Fig.3, and the DC  $v_M - i_M$  plot becomes Fig.4.

The bifurcation diagram and the Lyapunov exponent  $\lambda$  for  $C = 1, L = 3.3$  and  $\alpha = 0.2$  as a function of  $\beta$  are shown in Fig.4. The diagram shows that a bifurcation occurs at  $\beta = 1.23, 1.52$  and  $1.58$  and two circuits, four circuits and eight circuits, respectively appear.

The Fig.5 shows that in the region  $1.5 < \beta < 1.8$  the Lyapunov exponent  $\lambda$  is positive and about 0.04, and the bifurcation diagram is chaotic.

Ginoux, Letelier and Chua[16] calculated the flow curvature manifold of the memristor. Our result is consistent with their results.



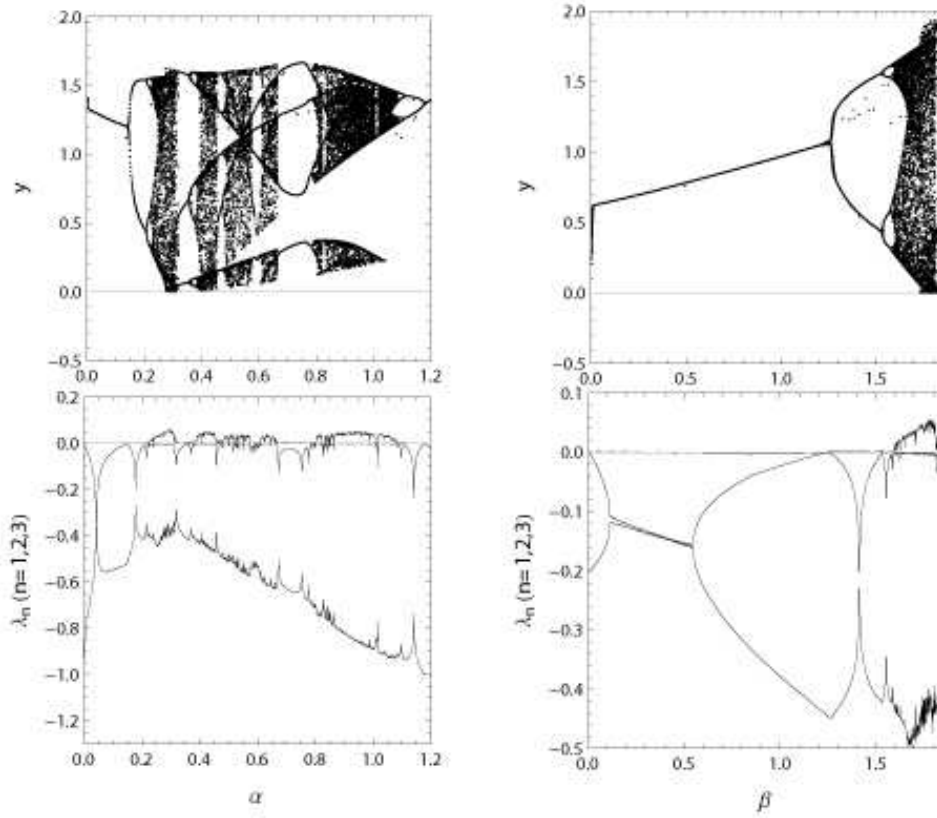


Figure 5: The bifurcation diagram and the Lyapunov exponent of Memristor.  $C=1, L=3.3$

## 4 Strange nonchaotic attractor in driven Muthuswamy-Chua's circuit

We added external input voltage  $F = \gamma \sin \omega t$  and consider the system of the equation

$$\begin{cases} \dot{x} = \frac{y}{C} \\ \dot{y} = \frac{-1}{L}[x + \beta(z^2 - 1)y + \gamma \sin \omega t] \\ \dot{z} = -y - \alpha z + yz \end{cases}$$

Strange nonchaotic attractor in periodically driven systems were investigated by Pikovsky and Feudel[27] and it was argued that without external oscillation, i.e. in autonomous systems it is difficult to find a SNA, but in periodically driven systems, SNAs had been observed. We want to investigate details of chaos and SNAs in driven MC circuits. When

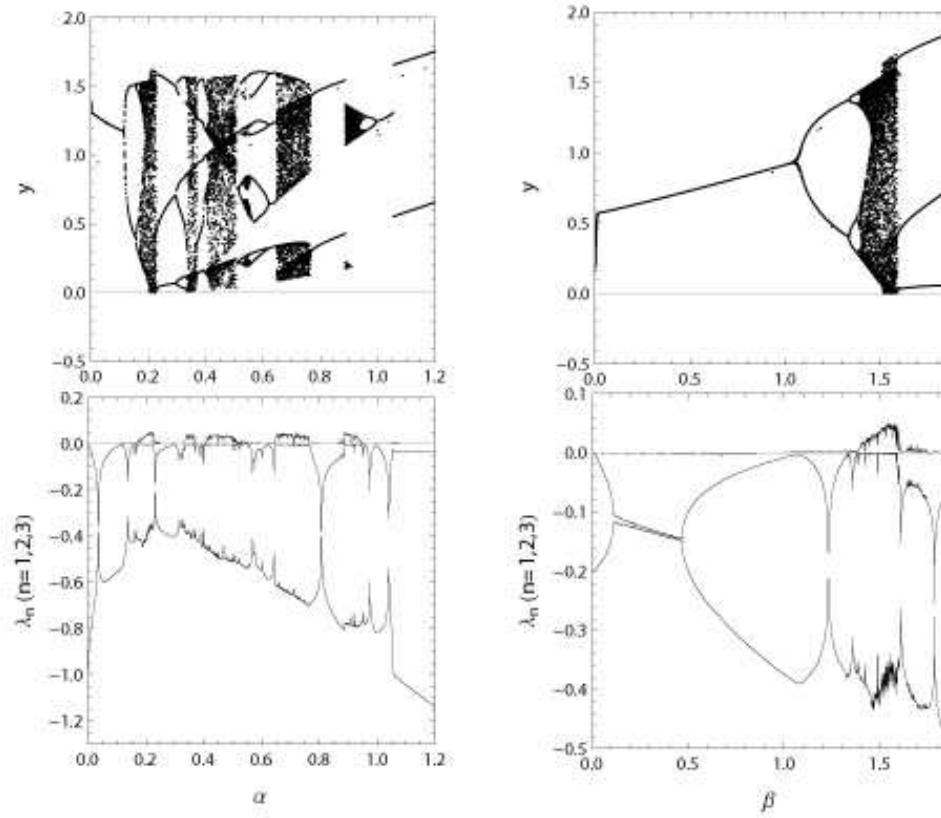


Figure 6: The bifurcation diagram and the Lyapunov exponent of Memristor.  $C = 1.2, L = 3.3$ .

$\gamma = 0.01$  i.e. very small, dependence of  $y$  as a function of  $\omega$  is chaotic. However, when we fixed  $C = 1.2$  and  $\gamma = 0.2$ , and modified  $\omega$  from 0.01 to  $\omega = 1$  we found a wide window of period 1 at around  $\omega = 0.51$ , as shown in Fig.8.

In the region  $0.51 \leq \omega \leq 0.62$  the period of the external voltage agrees with the eigenperiod of the system

$$\frac{1}{LC}T_s = \frac{1}{\sqrt{3.3}}T_s = 0.55T_s. \quad (9)$$

The corresponding frequency is  $f\omega T_s = 7.3\text{kHz}$  (8.8kHz in the case of  $C = 1$ ).

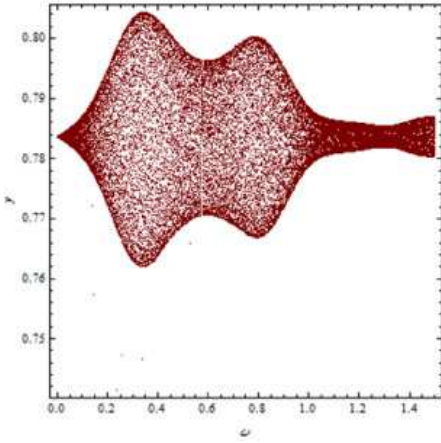


Figure 7: The bifurcation diagram  $C = 1, L = 3.3, \alpha = 0.2, \beta = 0.5, \gamma = 0.01$ .

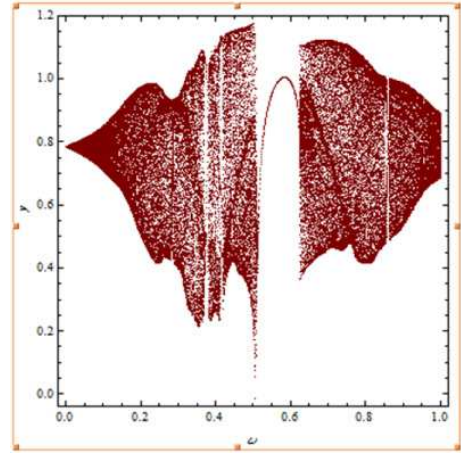


Figure 8: The bifurcation diagram  $C = 1, L = 3.3, \alpha = 0.2, \beta = 0.5, \gamma = 0.2$ .

We measured the bifurcation diagram and the Lyapunov exponents for the system with  $C = 1, L = 3.3, \alpha = 0.2, \beta = 0.5, \gamma = 0.2$  (Fig.8). We find non chaotic strange attractor in this case.

The bifurcation diagram for the system with  $C = 1.2, L = 3.3, \alpha = 0.2, \beta = 0.5, \gamma = 0.2$ , in the range  $0.24 \leq \omega \leq 0.36$  and  $0.36 \leq \omega \leq 0.46$  are shown in Fig.9 and in Fig.10, together with the frequency of the response  $f_d$ .

The Lyapunov exponent  $\lambda$  is calculated in Fig.11. When  $\omega \sim 0.3605$ ,  $\lambda$  becomes slightly positive up to about 0.01. The Lyapunov exponents are negative in the windows.

The frequency of the windows  $\omega$  as a function of the number of nodes of the response for

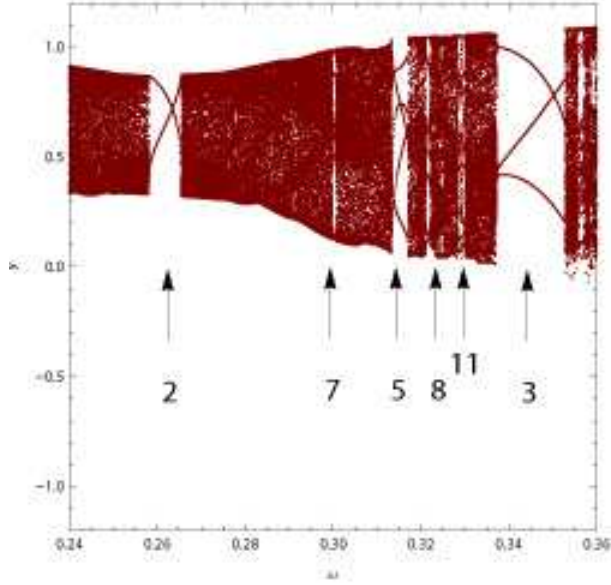


Figure 9: The bifurcation diagram of the driven memristor.  $C = 1.2, L = 3.3, 0.24 \leq \omega \leq 0.36$ .

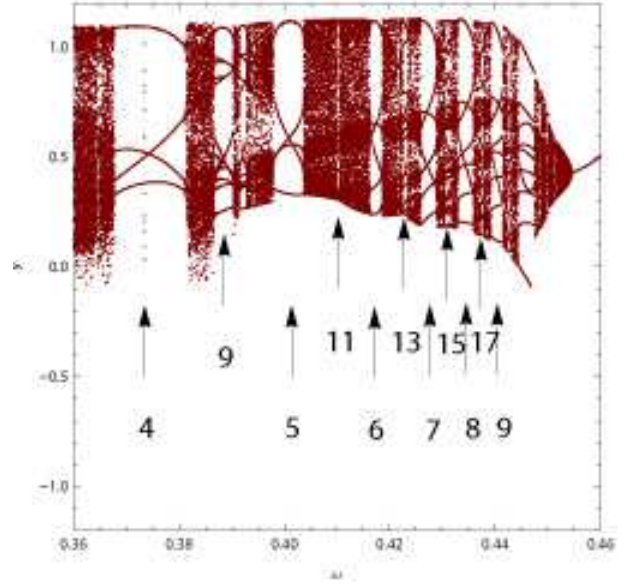


Figure 10: The bifurcation diagram of the driven memristor.  $C = 1.2, L = 3.3, 0.36 \leq \omega \leq 0.46$ .

samples of  $C = 1$  and  $C = 1.2$  are shown in Fig.12 and 13. In the case of one node, we put the  $\omega$  at  $f_d = 8$ , since when we put  $\omega/f_d$  as a function of the number of node  $f_d$ , the  $\omega$  of one node divided by 8 becomes close to that of node 7, as shown in Fig.14 and 15. The single period window may be considered as 8 degenerate nodes. The energy  $\omega/8$  of this node put at  $n = 8$  is consistent with  $\omega/f_d$  of  $f_d = 7$ , i.e. energy per node of  $f_d = \text{Mod}(-1, 8) = 7$ .

When  $C = 1$ , the matching  $\omega/f_d$  shifts about 10% lower than that of  $C = 1.2$ , and the width of the window is narrower than that of  $C = 1.2$ .

The attractor of  $n = 1$  of samples  $C = 1.2, L = 3.3$  at  $\omega = 0.51$  is shown in Fig.16, and the time series of  $x(t), y(t), z(t)$  are compared with  $\gamma \sin \omega t$  in Figs.17, 18, 19. Since the frequency of the response and that of driving term are both equal to 1, the ratio of  $W = f_s/f_d = 1/1$

At windows of node  $f_d = 2$  to  $f_d = 9$  of samples  $C = 1.2, L = 3.3$ , we compared the time sequence of the response and input  $\gamma \sin \omega t$ . Each time series  $x(t)$  are compared with

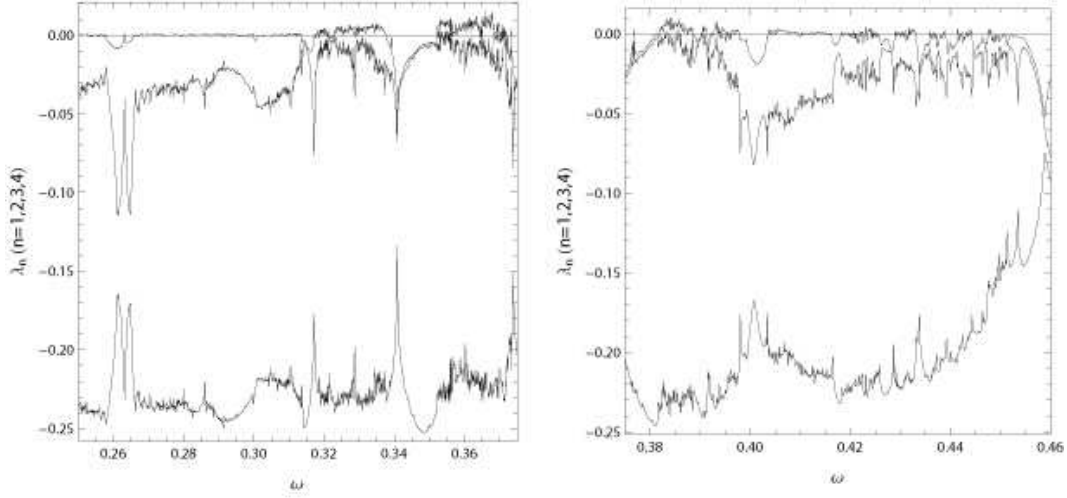


Figure 11: The Lyapunov exponent of Memristor.  $C = 1.2, L = 3.3, \alpha = 0.2, \beta = 0.5, \gamma = 0.2$ .

corresponding  $\gamma \sin \omega t$  and the ratio  $W = f_s/f_d$  are found to be

$$\left\{ \frac{1}{2}, \frac{2}{3}, \frac{3}{4}, \frac{4}{5}, \frac{5}{6}, \frac{6}{7}, \frac{7}{8}, \frac{8}{9}, \frac{1}{1} \right\}.$$

The sequence follows the period adding law[20]

$$\frac{q}{p} \rightarrow \frac{q+Q}{p+P} \rightarrow \frac{q+2Q}{p+2P} \rightarrow \dots \rightarrow \text{chaos} \rightarrow \frac{Q}{P}$$

The time series of  $x(t)$  and  $\gamma \sin \omega t$  at  $\omega = 0.4$ , which has  $W = 4/5$  is shown in Fig.20.

Between the window of  $f_d = 2$  and  $f_d = 3$ , we found a window of  $f_d = 5 = 2 + 3$ , which appears from the Farey sum

$$\frac{1}{2} + \frac{2}{3} \rightarrow \frac{3}{5}$$

A comparison of the time series  $x(t)$  and the corresponding  $\gamma \sin \omega t$  at  $\omega = 0.315$  allows the assignment  $W = 3/5$  as shown in Fig.21. This new node of  $W = 3/5$  and the node of  $W = 1/2$  makes a node of  $f_d = 7 = 5 + 2$ . A comparison of the time series  $x(t)$  and the corresponding  $\gamma \sin \omega t$  at  $\omega = 0.300$  allows the assignment  $W = 4/7$  as shown in Fig.22. The

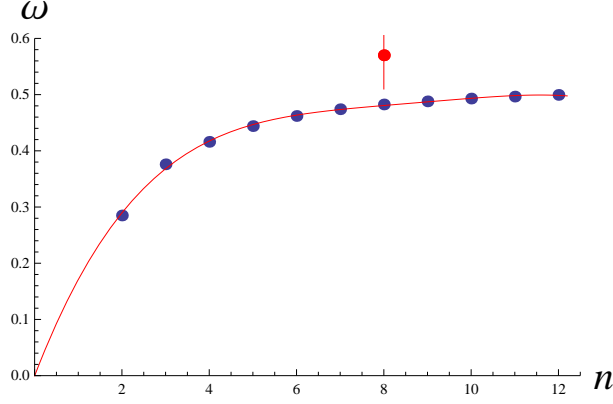


Figure 12: The fit of  $\omega$  as a function of torus loop  $n$ .  $C = 1.0$

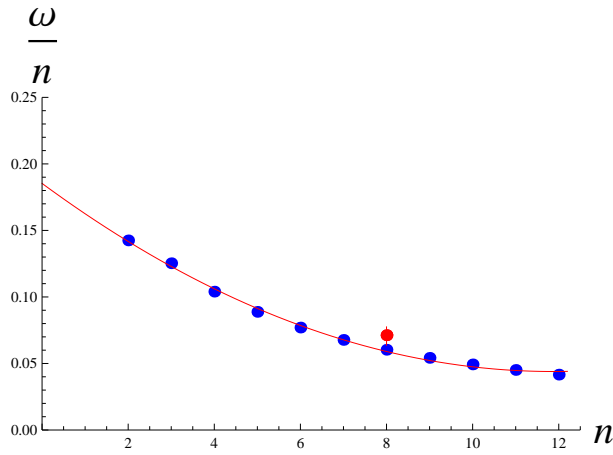


Figure 14: The fit of  $\omega/n$  as a function of the torus loop  $n$ .  $C = 1.0$

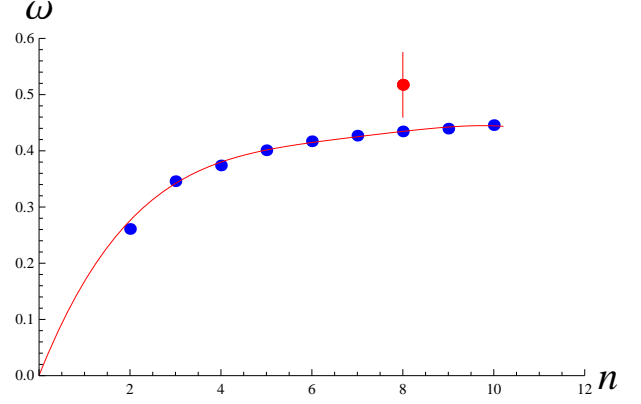


Figure 13: The fit of  $\omega$  as a function of torus loop  $n$ .  $C = 1.2$

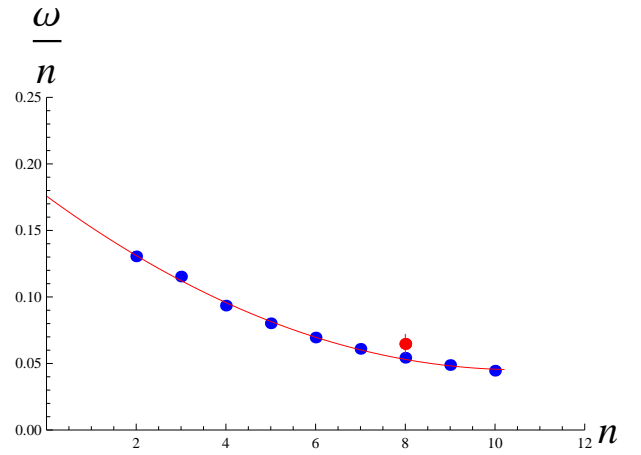


Figure 15: The fit of  $\omega/n$  as a function of torus loop  $n$ .  $C = 1.2$

new  $W$  again appears from the Farey sum

$$\frac{1}{2} + \frac{3}{5} \rightarrow \frac{4}{7}$$

The time series of  $x(t)$  and  $\gamma \sin \omega t$  of  $W = 6/7$  is shown in Fig.23 for comparison.

A similar comparison of  $W = \frac{2}{3} + \frac{3}{5} \rightarrow \frac{5}{8}$  and  $W = \frac{7}{8}$  is shown in Fig.24 and Fig.25 in the case of response  $f_d = 8$ , and a comparison of  $W = \frac{3}{4} + \frac{4}{5} \rightarrow \frac{7}{9}$  and  $W = \frac{8}{9}$  is shown in Fig.26 and Fig.27 in the case of response  $f_d = 9$ .

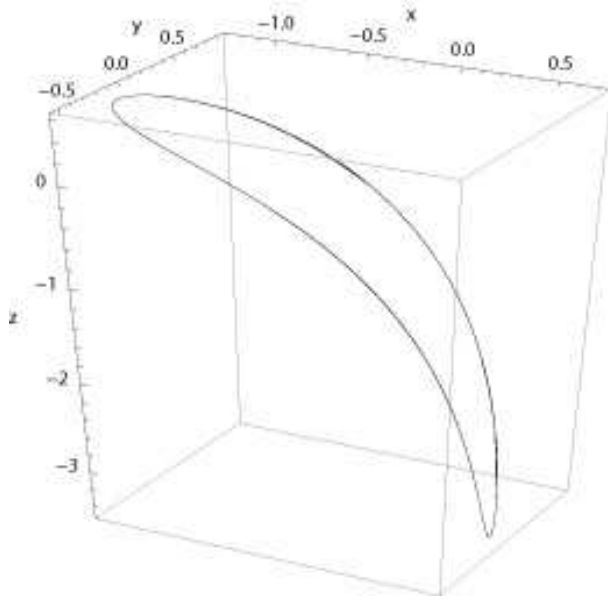


Figure 16: The attractor of  $f_d = 1$ .  $C = 1.2, L = 3.3, \alpha = 0.2, \beta = 0.5, \gamma = 0.2$

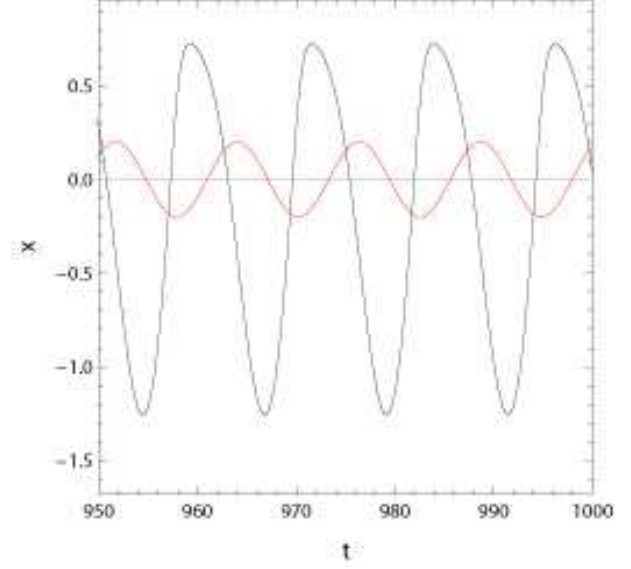


Figure 17: The time series of  $x(t)$  and  $\gamma \sin \omega t$ .  $\omega = 0.51, W = 1/1, C = 1.2, L = 3.3$

The series

$$\left\{\frac{3}{5}, \frac{4}{7}, \dots, \frac{1}{2}\right\}$$

follows the period adding law[20] with  $q = 3, Q = 1, p = 5, P = 2$ . The series

$$\left\{\frac{5}{8}, \frac{7}{9}, \dots, \frac{2}{1}\right\}$$

follows the period adding law with  $q = 5, Q = 2, p = 8, P = 1$ .

There are other Farey sums

$$\frac{4}{5} + \frac{5}{6} \rightarrow \frac{9}{11}, \quad \text{upto} \quad \frac{7}{8} + \frac{8}{9} \rightarrow \frac{15}{17}$$

from  $\omega = 0.41$  until  $\omega = 0.4375$ , which make the series of  $W$

$$\left\{\frac{9}{11}, \frac{11}{13}, \frac{13}{15}, \frac{15}{17}, \frac{2}{2}\right\}.$$

Near the region of  $\omega = 0.45$ , there is a window which has 10 nodes from left cluster and 9 nodes from right cluster as shown in Fig.10. We assign  $W = \{\frac{9}{9}, \frac{8}{8}, \frac{7}{7}\}$  at  $\omega = 0.446, 0.450$

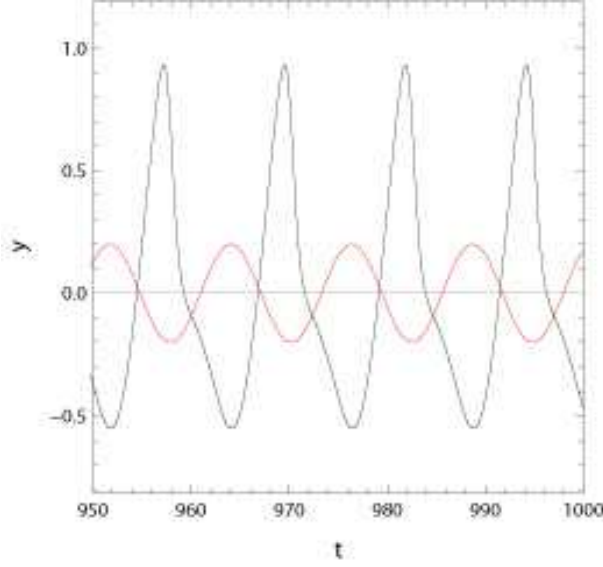


Figure 18: The time series of  $y(t)$  and  $\gamma \sin \omega t$ .  $\omega = 0.51, W = 1/1, C = 1.2, L = 3.3$

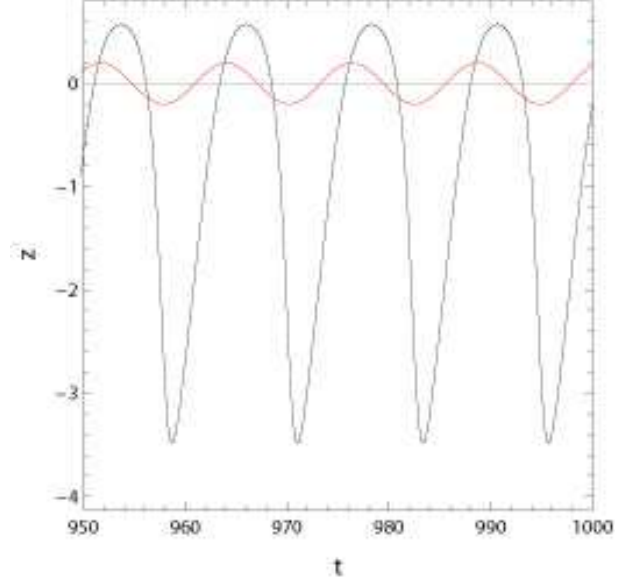


Figure 19: The time series of  $z(t)$  and  $\gamma \sin \omega t$ .  $\omega = 0.51, W = 1/1, C = 1.2, L = 3.3$

and 0.4515, respectively, and the Farey sums

$$\frac{8}{9} + \frac{9}{9} \rightarrow \frac{17}{18}, \quad \text{and} \quad \frac{9}{9} + \frac{8}{8} \rightarrow \frac{17}{17}$$

at  $\omega = 0.4425$  and  $\omega = 0.448$ , respectively.

The bifurcation diagram shows that when  $\omega = 0.3605$ , the system is chaotic. We studied Poincaré map of driven MC circuit at this  $\omega = 0.3605$  by taking the Poincaré map on the  $xy$  plane,  $yz$  plane and  $xz$  plane.

The points are plotted, when  $\omega t$  satisfies  $\text{Mod}[\omega t, 2\pi] = 0$ . We calculated the Poincaré map of  $\omega = 0.3605$  on  $xy, yz$  and  $xz$  plane, which are shown in Fig.28, 29 and 30.

In the case of oscillation on the  $xy$  plane, we calculated  $\Theta_n = \tan^{-1}(y_n/x_n)$ , where  $x_n$  and  $y_n$  are the  $x$  and  $y$  coordinates of the Poincaré map. The return map of  $\Theta_{n+1}$  v.s.  $\Theta_n$  simplifies the chaotic behaviors (Fig.31). It becomes a single line in the case of  $\omega < 0.26$ , four clusters when  $\omega = 0.3$ , and chaotic when  $\omega = 0.32$  as shown in Fig.32. When  $\omega = 0.5$ , clusters appear again, and when  $\omega = 0.6$ , a single line appears again as shown in Fig.33 .



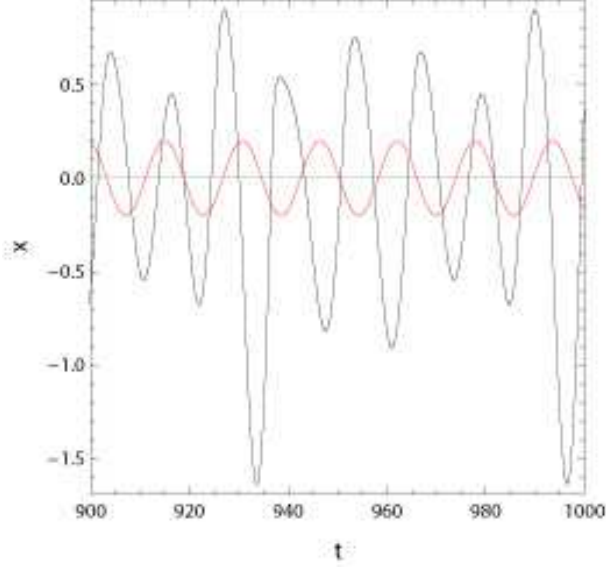


Figure 20: The time series of  $x(t)$  and  $\gamma \sin \omega t$ .  $\omega = 0.40, W = 4/5, C = 1.2, L = 3.3$

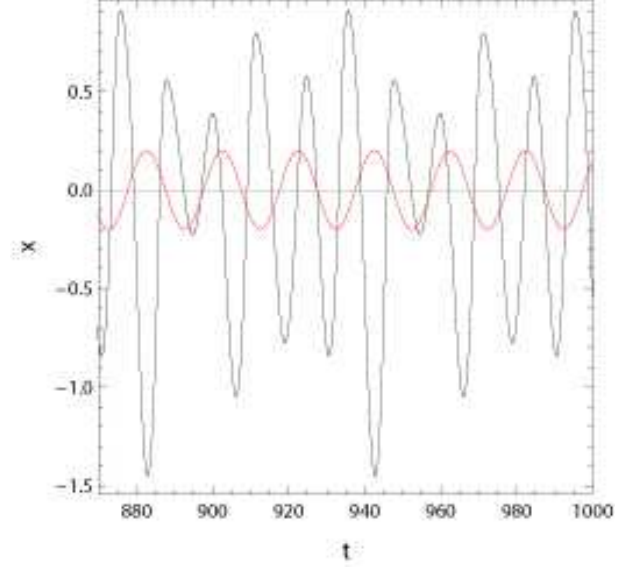


Figure 21: The time series of  $x(t)$  and  $\gamma \sin \omega t$ .  $\omega = 0.315, W = 3/5, C = 1.2, L = 3.3$

We observed that except near  $\omega = 0.36$ ,  $\lambda$  is negative, and the oscillation is non-chaotic in most regions.

In the case of  $C = 1.2$ , we observed Windows= $\{\frac{1}{2}, \dots, \frac{8}{9}\}$ , i.e. 8 levels were observed, (The level  $\frac{9}{10}$  is broken in the high frequency part.) and above the level  $\frac{4}{5}$  the level  $\frac{7}{9}$  in the Farey sequence  $\{\frac{3}{4}, \frac{7}{9}, \frac{4}{5}\}$  is made and the sequence  $\{\frac{9}{11}, \dots, \frac{15}{17}\}$  follows.

Below the level  $\frac{9}{9}$  the Farey sequence are different, and as the source of 8 levels in the  $C = 1.2$  case, we imagine a combination of the input electron and the output electron both expressed by quaternions. Two quaternions can make an octonion which couples with 8 dimensional vector fields.

In the case of  $C = 1.0$  and  $\gamma = 0.2$ ,  $\omega$  of the node  $W = \frac{1}{1}$  is about 10% larger than that of  $C = 1.2$ , and the node  $n$  at highest  $\omega$  was assigned up to 15, in contrast to up to 8 in the case of  $C = 1.2$ .

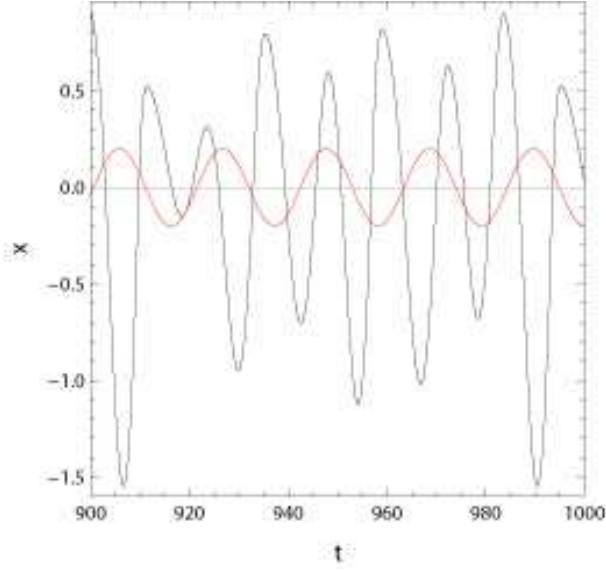


Figure 22: The time series of  $x(t)$  and  $\gamma \sin \omega t$ .  $\omega = 0.30, W = 4/7, C = 1.2, L = 3.3$

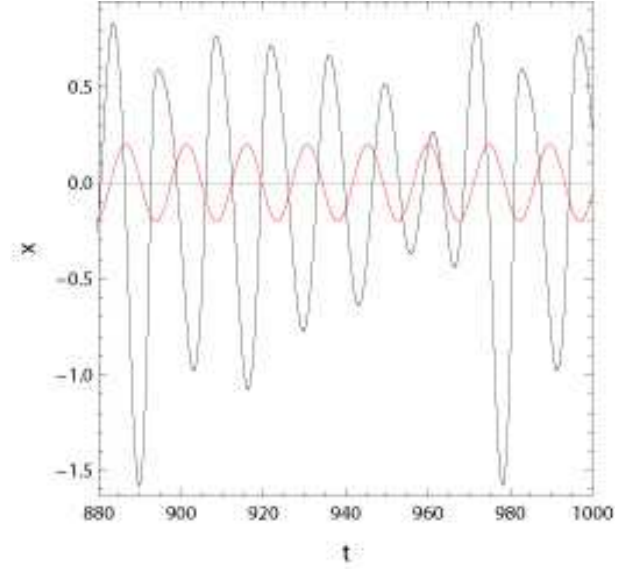


Figure 23: The time series of  $x(t)$  and  $\gamma \sin \omega t$ .  $\omega = 0.427, W = 6/7, C = 1.2, L = 3.3$

The width of the windows is narrower, and the sequences of  $W$  consist of

$$\left\{ \frac{1}{2}, \frac{2}{3}, \frac{3}{4}, \frac{4}{5}, \frac{5}{6}, \frac{6}{7}, \frac{7}{8}, \frac{8}{9}, \frac{9}{10}, \frac{10}{11}, \frac{11}{12}, \frac{12}{13}, \frac{13}{14}, \frac{14}{15}, \frac{1}{1} \right\}.$$

The Farey sequences of  $P \neq Q$  like  $W = \left\{ \frac{3}{5}, \frac{4}{7} \right\}$  and  $W = \left\{ \frac{5}{8}, \frac{7}{9} \right\}$ , which were observed in  $C = 1.2$ , were not observed in  $C = 1.0$ .

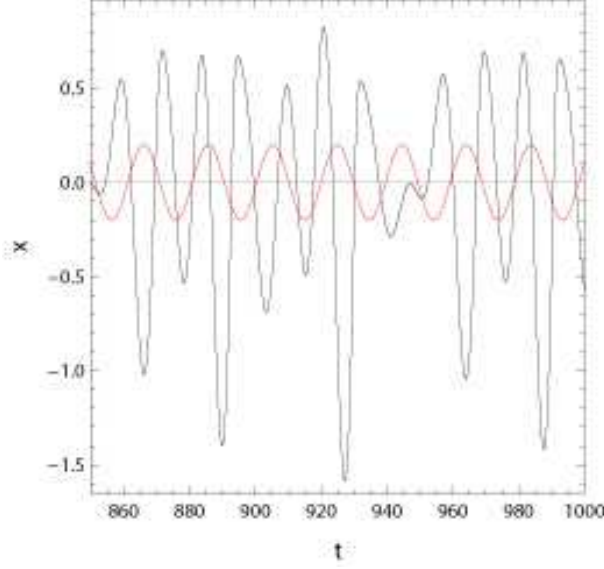


Figure 24: The time series of  $x(t)$  and  $\gamma \sin \omega t$ .  $\omega = 0.321, W = 5/8, C = 1.2, L = 3.3$

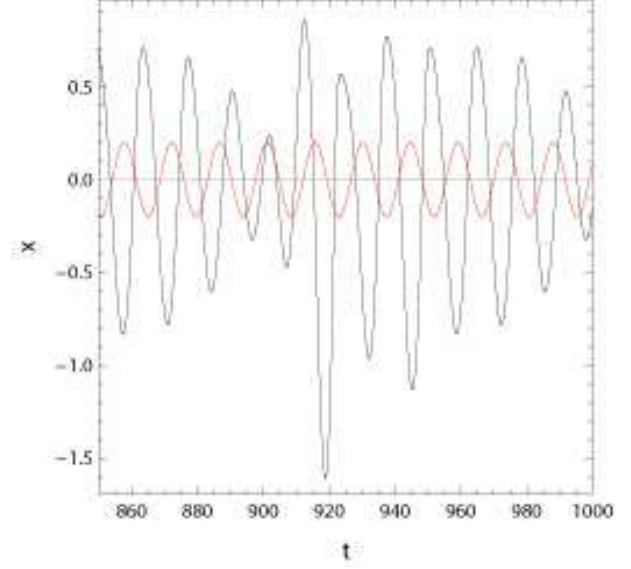


Figure 25: The time series of  $x(t)$  and  $\gamma \sin \omega t$ .  $\omega = 0.434, W = 7/8, C = 1.2, L = 3.3$

## 5 Conjecture on the frequency of the windows of driven Muthuswamy-Chua's circuit

The four component Dirac's spinor is a combination of two two-component spinors each transforms as a quaternion. É. Cartan[28] defined, using semi-spinors of an even number of indices

$$\xi_{even} := \xi_{12}, \xi_{23}, \xi_{34}, \xi_{13}, \xi_{24}, \xi_{14}, \xi_{1234}, \xi_0$$

and semi-spinors of an odd number of indices

$$\xi_{odd} := \xi_1, \xi_2, \xi_3, \xi_4, \xi_{234}, \xi_{134}, \xi_{124}, \xi_{123},$$

four bases of spinors

In octonion basis, we consider a fermion  $\phi$  and its charge conjugate  $C\phi$ , which are de-

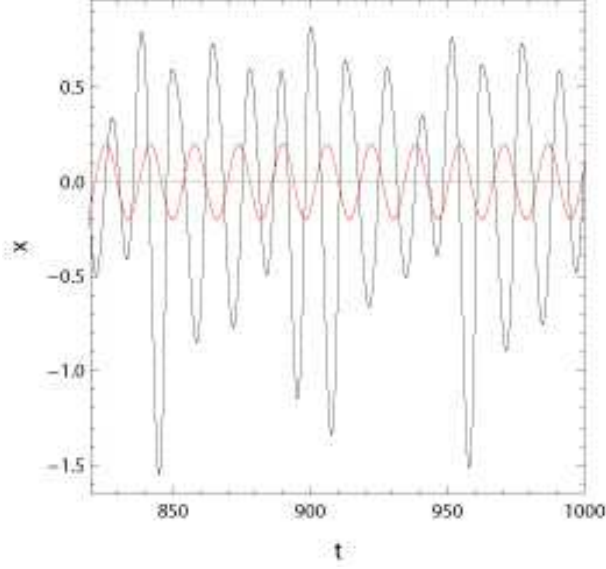


Figure 26: The time series of  $x(t)$  and  $\gamma \sin \omega t$ .  $\omega = 0.39, W = 7/9, C = 1.2, L = 3.3$

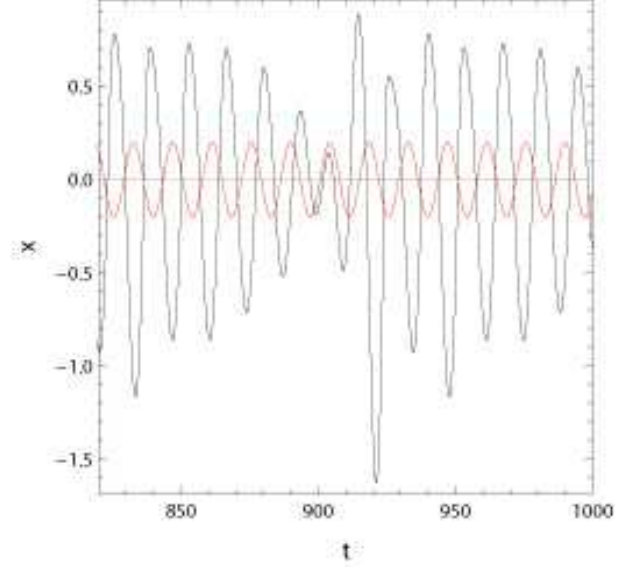


Figure 27: The time series of  $x(t)$  and  $\gamma \sin \omega t$ .  $\omega = 0.44, W = 8/9, C = 1.2, L = 3.3$

scribed by

$$\mathcal{A} = \xi_0 I + \xi_{14} \sigma_x + \xi_{24} \sigma_y + \xi_{34} \sigma_z = \begin{pmatrix} A_4 + i A_3 & i A_1 - A_2 \\ i A_1 + A_2 & A_4 - i A_3 \end{pmatrix}$$

$$\mathcal{B} = \xi_{1234} I - \xi_{23} \sigma_x - \xi_{31} \sigma_y - \xi_{12} \sigma_z = \begin{pmatrix} B_4 - i B_3 & -i B_1 + B_2 \\ -i B_1 - B_2 & B_4 + i B_3 \end{pmatrix}$$

and anti-fermion  $\psi$  and its charge conjugate  $C\psi$ , which are described by

$$\mathcal{C} = \xi_4 I + \xi_1 \sigma_x + \xi_2 \sigma_y + \xi_3 \sigma_z = \begin{pmatrix} C_4 + i C_3 & i C_1 - C_2 \\ i C_1 + C_2 & C_4 - i C_3 \end{pmatrix}$$

$$\mathcal{D} = \xi_{123} I - \xi_{234} \sigma_x - \xi_{314} \sigma_y - \xi_{124} \sigma_z = \begin{pmatrix} D_4 - i D_3 & -i D_1 + D_2 \\ -i D_1 - D_2 & D_4 + i D_3 \end{pmatrix}.$$

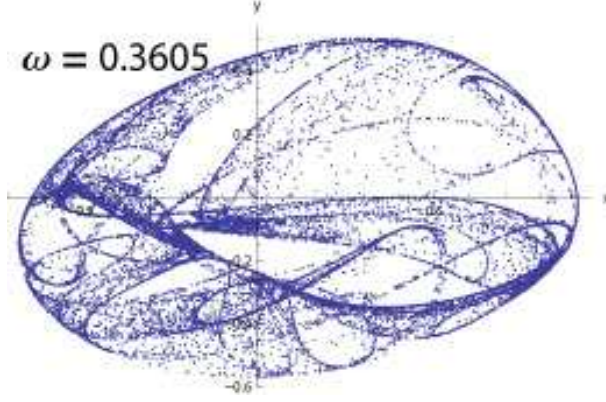


Figure 28: The Poincaré map on the  $xy$  plane.  $\omega = 0.3605$ .

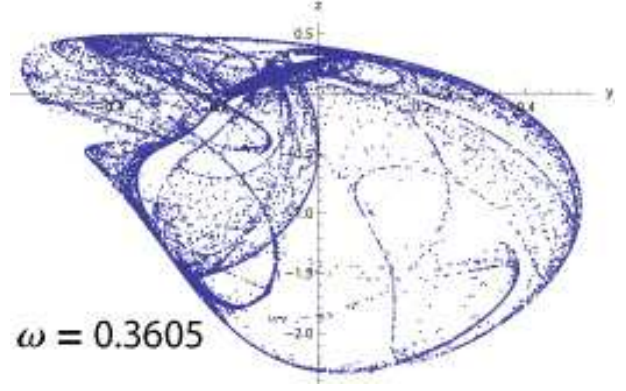


Figure 29: The Poincaré map on the  $yz$  plane.  $\omega = 0.3605$ .

The coupling of the spinor and vectors defined by Cartan is

$$\begin{aligned}
\mathcal{F} &= {}^t\phi CX\psi = x^1(-A_1D_2 - B_2D_3 + B_3D_4 + B_4C_1) \\
&+ x^2(B_1D_3 - A_2D_4 - B_3D_1 + B_4C_2) \\
&+ x^3(-B_1D_2 + B_2D_1 - A_3D_4 + B_4C_3) \\
&+ x^4(-A_1D_1 - A_2D_2 - A_3D_3 + B_4C_4) \\
&+ x^{1'}(B_1C_4 - B_2C_3 - B_3C_2 - A_4D_1) \\
&+ x^{2'}(A_1C_3 + B_2C_4 - A_3C_1 - A_4D_2) \\
&+ x^{3'}(-A_1C_2 + A_2C_1 + B_3C_4 - A_4D_3) \\
&+ x^{4'}(-B_1C_1 - B_2C_2 - B_3C_3 + A_4D_4)
\end{aligned}$$

In our system, there are an input electron which is represented by the plane wave, and an output fermion. There are 4 possible choice of the input fermion wave functions  $\mathcal{A}, B, C, D$ , and 2 possible types of exchanged photon i.e. left vertex and right vertexs are the same  $x_4$  or  $x'_4$  exchange, and left vertexis  $x_4$  and right vertex is  $x'_4$  or vice versa, which we denote  $x_4/x'_4$  exchange. Thus, there are 8 types of interactions.

The exchange of  $x_4$  between a particle  $\tilde{\mathcal{A}} = \begin{pmatrix} B_4 + i A_3 & i A_1 - A_2 \\ i A_1 + A_2 & B_4 - i A_3 \end{pmatrix} = (\vec{A}, B_4)$  and

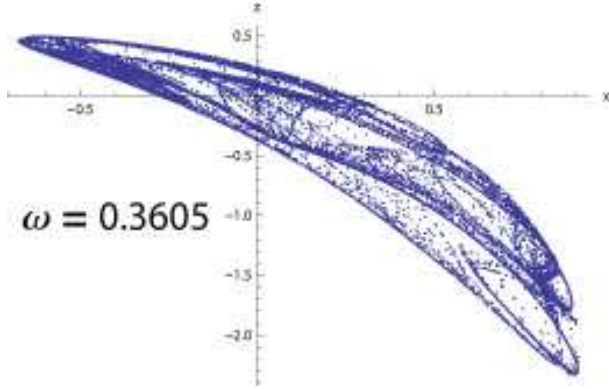


Figure 30: The Poincaré map on the  $xz$  plane.  $\omega = 0.3605$ .

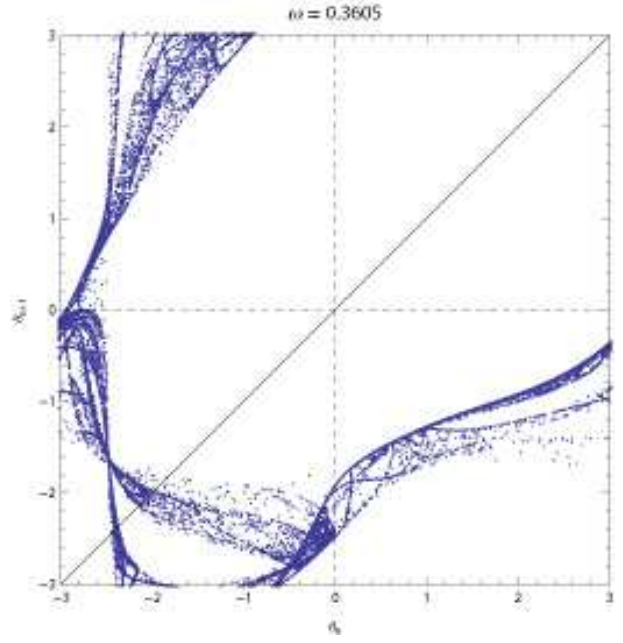


Figure 31: The  $\Theta$  angle of the Poincaré map on the  $xy$  plane.  $\omega = 0.3605$ .

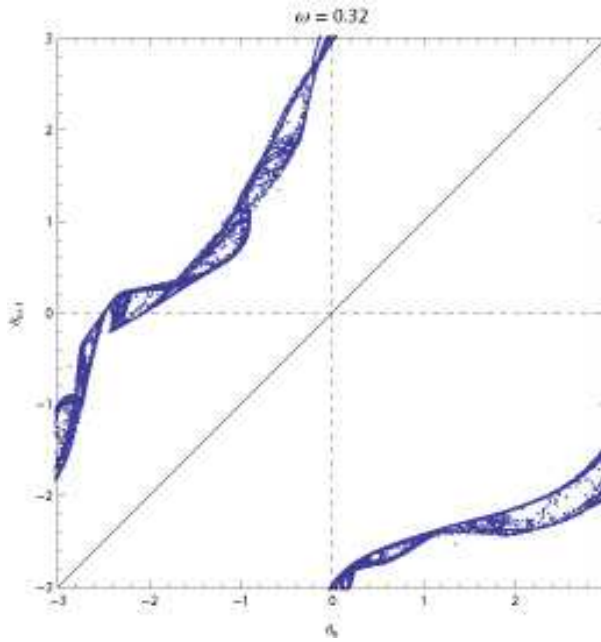


Figure 32: The  $\Theta$  angle of the Poincaré map on the  $xy$  plane.  $\omega = 0.32$ .

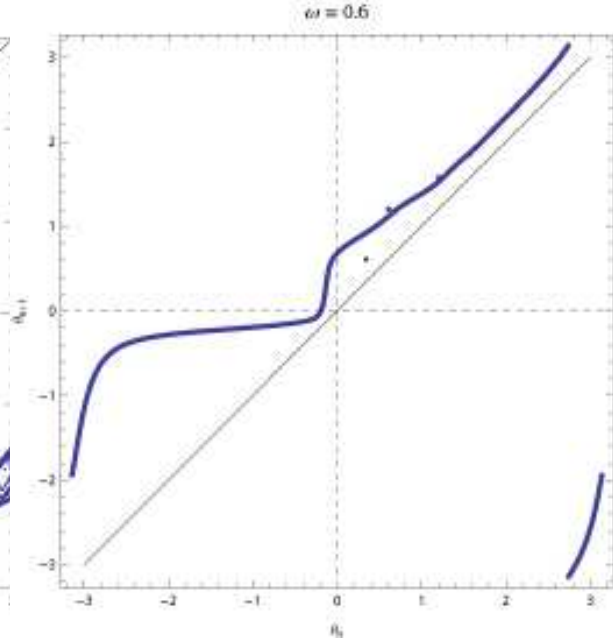


Figure 33: The  $\Theta$  angle of the Poincaré map on the  $xy$  plane.  $\omega = 0.60$ .

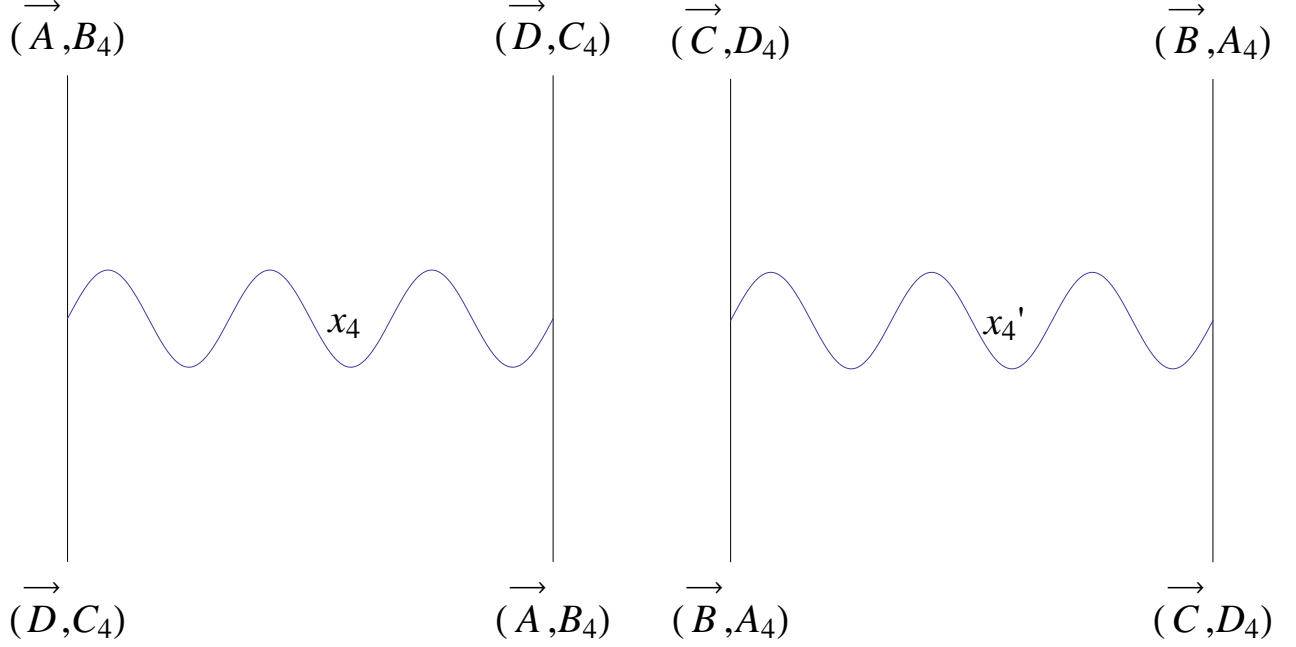


Figure 34: The vector  $x_4$  exchange between particle-particle  $(\vec{D}, C_4), (\vec{A}, B_4)$ .

Figure 35: The vector  $x'_4$  exchange between hole-hole  $(\vec{B}, A_4), (\vec{C}, D_4)$ .

another particle  $\tilde{D} = \begin{pmatrix} C_4 + i D_3 & i D_1 - D_2 \\ i D_1 + D_2 & C_4 - i D_3 \end{pmatrix} = (\vec{D}, C_4)$  is represented in Fig.34.

The exchange of  $x'_4$  between a hole  $\tilde{B} = \begin{pmatrix} A_4 + i B_3 & i B_1 - B_2 \\ i B_1 + B_2 & A_4 - i B_3 \end{pmatrix} = (\vec{B}, A_4)$  and another hole  $\tilde{C} = \begin{pmatrix} D_4 + i C_3 & i C_1 - C_2 \\ i C_1 + C_2 & D_4 - i C_3 \end{pmatrix} = (\vec{C}, D_4)$  is represented in Fig.35.

Since the vector particle is assumed to be self-dual, or propagation of  $x_4$  is same as that of  $x'_4$ , the hole-particle interaction between  $(\vec{C}, D_4)$  and  $(\vec{A}, B_4)$  represented in Fig.36, and the particle-hole interaction between  $(\vec{D}, C_4)$  and  $(\vec{B}, A_4)$  represented in Fig.37 are possible.

Our analysis of MC circuit we define the voltage across the capacitor  $x_1 = v_C(t)$ , the current through the inductor  $x_2 = i_L(t)$  and the internal state of the memristor  $x_3 = z(t)$ .

From the frequency  $\omega$  of the single period oscillation observed in the widest window of

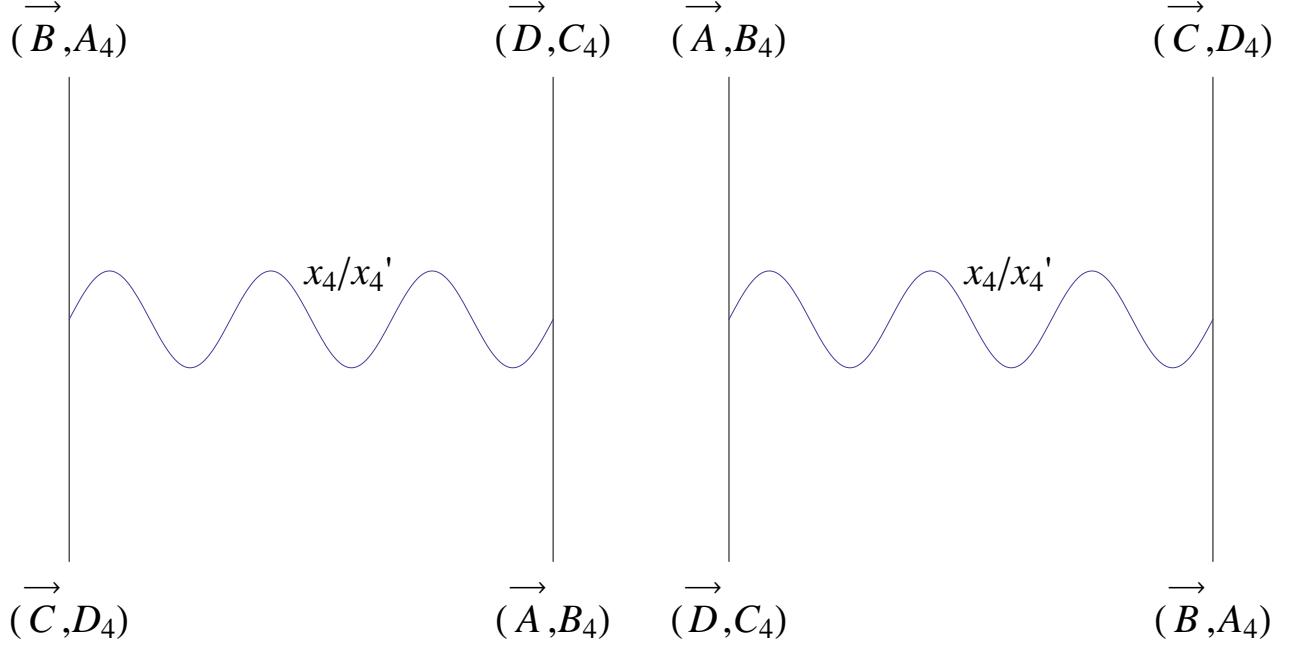


Figure 36: The vector  $x_4/x_4'$  exchange between hole-particle  $(\vec{C}, D_4), (\vec{A}, B_4)$

Figure 37: The vector  $x_4/x_4'$  exchange between particle-hole  $(\vec{D}, C_4), (\vec{B}, A_4)$

the bifurcation diagram, we calculate  $\omega/8$  and compare the  $\omega/n$  of oscillation of periodicity equals to  $n$ . The Figs.15 and 14 show a three periodic oscillations around  $\omega = 0.375$ ,  $\omega/3 = 0.125$ , a four periodic oscillations around  $\omega = 0.416$ ,  $\omega/4 = 0.104$ , and a five periodic oscillation around  $\omega = 0.444$ ,  $\omega/5 = 0.088$ .  $\omega$  divided by a number of periods  $n$  defined as  $\omega/n$  is nearly linear function of  $0.18 - 0.018n$ . In the case of  $C = 1.2$ , we observe windows of periodicity  $n = 2$  to 9. The last window of periodicity 10 is broken at the high frequency region. In the case of  $C = 1.2$ , we observed windows of  $n = 2, \dots, 9$ , which have the smooth dependence of  $\omega/n$ . In the case of  $C = 1$ , we observed windows of  $n = 2, \dots, 15$ , which have the same behavior.

The 2nd order particle-particle or hole-hole interaction occurs through the Figs.38 and 39.

The particle-hole interaction is possible through double vector  $x_4/x_4'$  exchange shown in Figs.40 and 41.



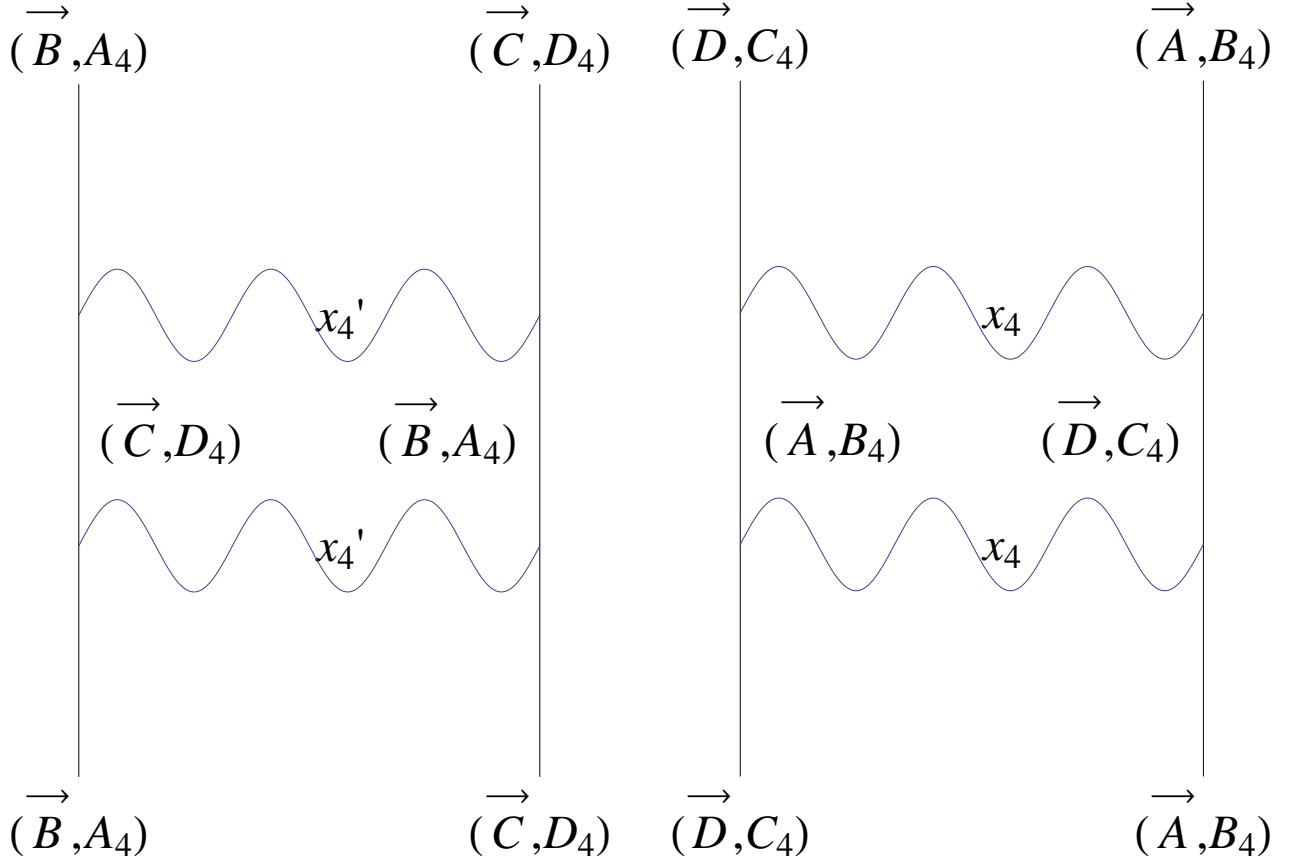


Figure 38: The double vector  $x_4$  exchange between hole-hole  $(\vec{B}, A_4), (\vec{C}, D_4)$ .

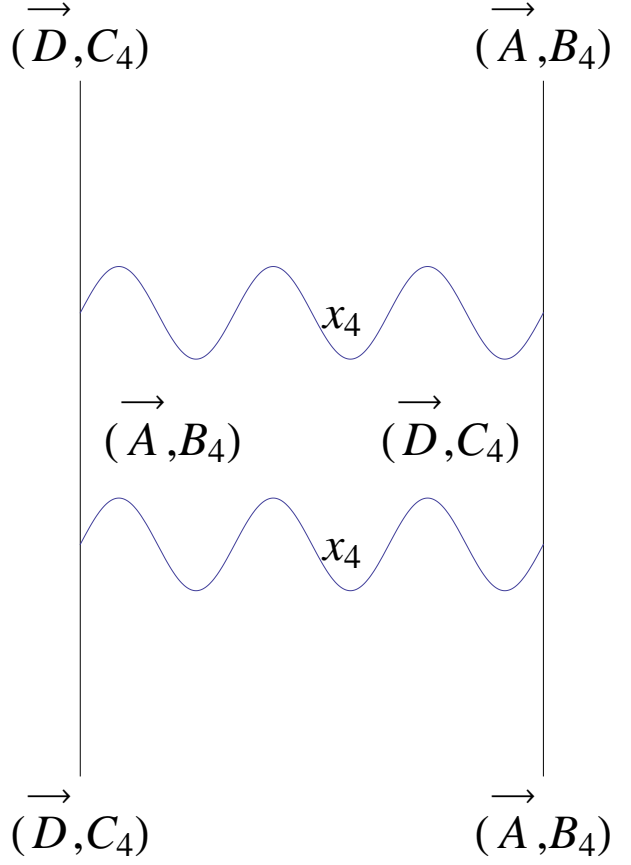


Figure 39: The double vector  $x_4'$  exchange between particle-particle  $(\vec{D}, C_4), (\vec{A}, B_4)$ .

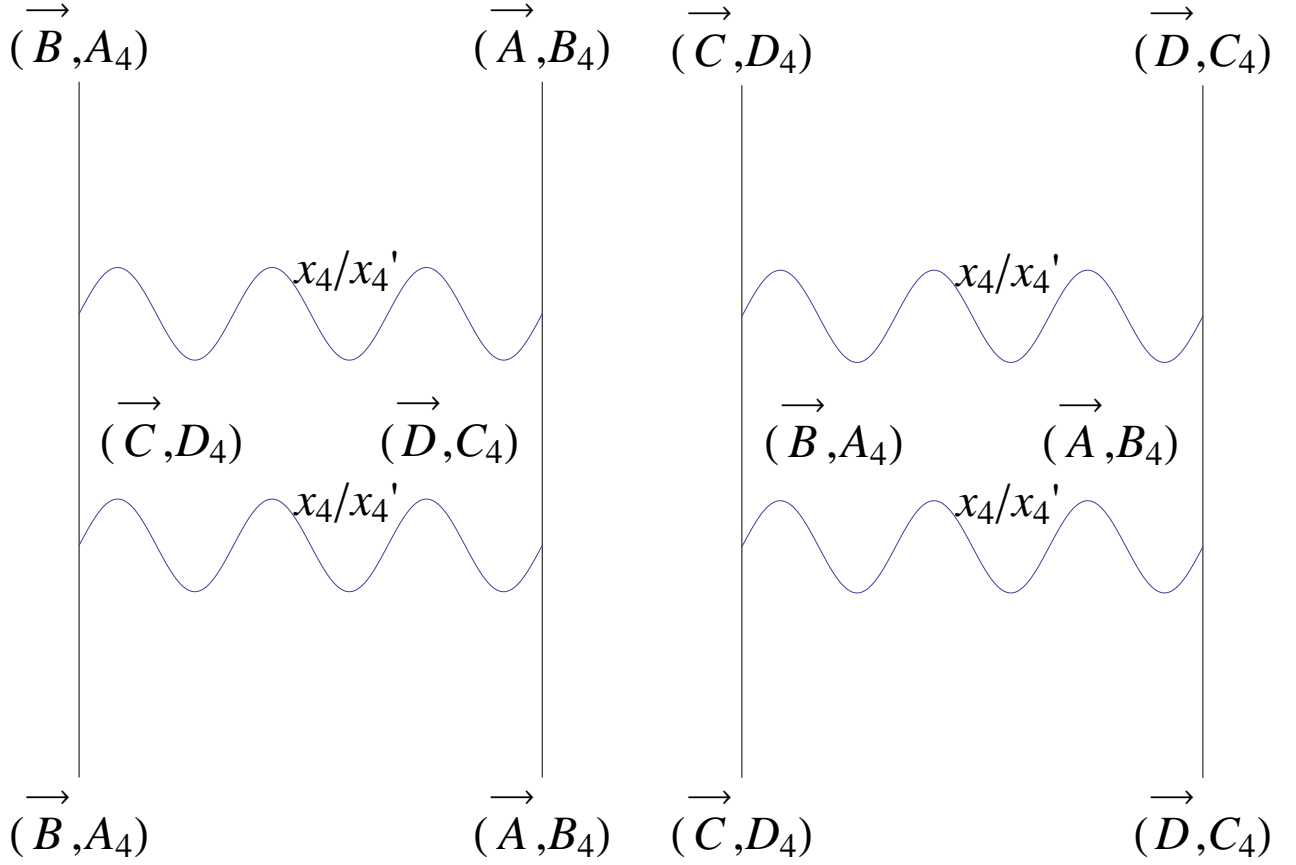


Figure 40: The double vector  $x_4/x_4'$  exchange between hole-particle  $(\vec{B}, A_4), (\vec{A}, B_4)$ .

Figure 41: The double vector  $x_4/x_4'$  exchange between hole-particle  $(\vec{C}, D_4), (\vec{D}, C_4)$ .

## 6 Discussion

We studied the sinusoidally driven memristor circuit. We observed non chaotic strange attractors and different from the case of driven Chua's circuit[20], we first observed period adding low as in LCR circuit[22]. In the case of  $C = 1.2$ , we observed a sequence of response frequency  $f_d$  stepwise increasing, and the winding number  $W = f_s/f_d$  shows a sequence  $W = \{\frac{1}{2}, \frac{2}{3}, \frac{3}{4}, \dots, \frac{8}{9}, \frac{1}{1}\}$  and Farey sum sequences  $W = \{\frac{3}{5}, \frac{4}{7}, \dots, \frac{1}{2}\}$  and  $\{\frac{5}{8}, \frac{7}{9}, \dots, \frac{2}{1}\}$ . It is interesting that in the analysis of non-linear circuit of [21], the number of response  $P$  of the  $v_C$ , which corresponds to our  $f_d$ , was assigned as Level-2 devil's staircase sequence from step 2, and 8 steps  $P = 2, 3, \dots, 9$  were considered as in our case of  $C = 1.2$ .

In the case of  $C = 1$ , we find winding number sequences  $W = \{\frac{1}{2}, \frac{2}{3}, \frac{3}{4}, \dots, \frac{14}{15}, \frac{1}{1}\}$ , but we do not find the Farey sum sequences observed in  $C = 1.2$ . It means that the way to chaos via devil's staircase which is observed in the case of  $C = 1.2$  is absent in the case of  $C = 1$ . The sequence of  $W$  can be decomposed as 8 steps  $W = \{\frac{2}{3}, \frac{4}{5}, \frac{6}{7}, \frac{8}{9}, \frac{10}{11}, \frac{12}{13}, \frac{14}{15}, \frac{2}{1}\}$  and 8 steps  $W = \{\frac{1}{2}, \frac{3}{4}, \frac{5}{6}, \frac{7}{8}, \frac{9}{10}, \frac{11}{12}, \frac{13}{14}, \frac{2}{1}\}$ , but the limit  $W = 1$  is common, and so there are altogether 15 steps in the case of  $C = 1$ . In the Level-2 devil's staircase sequence from step 3 to step 2 of [21], 7 steps  $P = 3, 5, \dots, 15$  were considered.

When  $\omega$  of  $W = 1$  is divided by 8, it becomes close to  $\omega$  of  $W = \frac{6}{7}$  divided by 7. It suggests that the octonion that appears as a combination of two quaternions plays an important role in the circuit, since Dirac electrons are expressed by quaternions.

Oscillation in the voltage of two capacitances  $v_{C1}, v_{C2}$  and the current  $i_L$  of an inductor in nonlinear coupled circuits can be analyzed using the quaternion bases. In MC circuits, octonion plays an important role in the matching of period  $\omega/f_d$ . Symmetry of electromagnetic field and that of probes must be studied together. We found nonchaotic strange attractors, or strange attractors whose Lyapunov exponent is negative, in the driven MC circuit.

The Poincaré map of the memristor current obtained by choosing the plane defined by the condition  $Mod[\omega t, 2\pi] = 0$  shows a relatively complicated structure at a certain frequency

region. When the amplitude of the external oscillation is small, the strange attractor remains nonchaotic, but when it is large, the strange attractor at a certain frequency region becomes chaotic. The condition depends upon the capacity of the condenser  $C$ .

We considered vector particle interactions with electron particles and holes which are represented by octonions. We can extend the theory to electrons and positrons represented by octonions, and furthermore quarks and anti-quarks represented by octonions[29, 30]. The details will be discussed elsewhere.

S.F. thanks Dr. F. Nakamura of Wolfram Research for a support in programming using Mathematica 9.

## References

- [1] S. Hayes, C. Grebogi and E. Ott, Communicating with Chaos, Rev. Mod. Phys. **70**, 2031-2034 (1993).
- [2] J.-P. Eckman and D. Ruelle, Ergodic theory of chaos and strange attractors, Rev. Mod. Phys. **57**, 617 (1985).
- [3] P. Grassberger and I. Procaccia, Measuring the Strangeness of Strange Attractors, Physica **9D** (1983).
- [4] C. Grebogi, E. Ott, S. Pelikan and J.A. Yorke, Strange Attractors that are not Chaotic, Physica **13D**, 261(1984).
- [5] M. Ding, C. Grebogi and E. Ott, Dimension of Strange Nonchaotic Attractors, Phys. Lett. A **137**, 167 (1989).
- [6] J.F. Heagy and S.M. Hammel, The birth of strange nonchaotic attractors, Physica **D70** 140-153 (1994).
- [7] G. Keller, A note on strange nonchaotic attractors, Fundamenta Mathematicae **151**, 139 (1996).
- [8] P. Grendinning, Global attractors of pinched skew products, Dynamical Systems **17**, 287 (2002).
- [9] L. Alsedà and M. Misiurewicz, Attractors for unimodal quasiperiodically forced maps, Journal of Difference Equations and Applications, **14** 1175 (2008).
- [10] M. Gröger and T. Jäger, Dimension of Attractors in Pinched Skew Products, arXiv:1111.6574 v2[math.DS](2013).
- [11] L.O. Chua, Memristor-The Missing Circuit Element, IEEE Transactions on Circuit Theory, **CT-18**, 507 (1971).

- [12] L.O.Chua and S.M. Kang, Memristive Devices and Systems, Proceedings of the IEEE, **64**, 209 (1976).
- [13] B. Muthuswamy and L.O. Chua, Simplest Chaotic Circuit, International Journal of Bifurcation and Chaos, **20**, 1567 (2010).
- [14] J.-M. Ginoux and Ch. Letellier, Flow curvature manifolds for shaping chaotic attractors: I. Rössler-like systems, J. Phys. A: Math. Theor. **42**, 285101-17 (2009).
- [15] R. Gilmore, J-M. Ginoux, T. Jones, C. Letellier and U.S. Freitas, Connecting curves for dynamical systems, J. Phys. A: Mathe Theor. **43**, 255101-13 (2010).
- [16] J.M. Ginoux, Ch. Letellier and L.O. Chua, Topological Analysis of Chaotic Solution of Three-Element Memristive Circuit, International Journal of Bifurcation and Chaos **20**,3819-3827 (2010).
- [17] L.O. Chua, Resistance switching memories are memristors, Appl. Phys. **A 102**, 765-783 (2011).
- [18] L.O. Chua, Komuro and Matsumoto, The Double Scroll Family, IEEE Transactions on Circuit Theory, (1986).
- [19] T. Saito and H. Nakano, Chaotic Circuits Based on Dependent Switched Capacitors, CP676 Experimental Chaos, AIP Proceedings, 3-13 (2003).
- [20] L. Pivka, A.L. Zheleznyak and L.O. Chua, Arnold's Tongues, Devil's Staircase and Self-similarity in the Driven Chua's Circuit, International Journal of Bifurcation and Chaos **20**,1743-1753 (1994).
- [21] L.O. Chua, Y. Yao and Q. Yang, Devil's Staircase Route to Chaos in a Non-Linear Circuit, Circuit Theory and Applications, **14**, 315-329 (1986).

- [22] I. Manimehan, K. Thamilmaran, G. Chidambaram and P. Philominathan, Transition From Torus To Chaos In A Piecewise-linear Forced Parallel LCR Circuit, National Conference on Nonlinear Systems & Dynamics, 1-4 (2005).
- [23] Z. Zhu and Z. Liu, Strange Nonchaotic Attractors of Chua's Circuit with Quasiperiodic Excitation, International Journal of Bifurcation and Chaos, **7**, 227-238 (1997).
- [24] M.S. Baptista and I.L. Cardas, Phase-Locking and Bifurcations of the Sinusoidally-Driven Double Scroll Circuit, Nonlinear Dynamics **17**, 119-139 (1998)
- [25] K. Thamilmaran and M. Lakshmanan, Classification of Bifurcations and Routes to Chaos in a Variant of Murali-Lakshmanan-Chua Circuit, International Journal of Bifurcation and Chaos **12**, 783-813 (2002).
- [26] S. Furui and S. Niiya, Shil'nikov chaos control using homoclinic orbits and the Newhouse region, Chaos, Solitons and Fractals, **34**, 966-988 (2007).
- [27] A. Pikovsky and U. Feudel, Comment on "Strange nonchaotic attractors in autonomous and periodically driven system", Phys. Rev. E, **56**, 7320-7321 (1997).
- [28] É. Cartan, "The Theory of Spinors", Dover Pub. (1966).
- [29] S.Furui, Fermion Flavors in Quaternion Basis and Infrared QCD, Few-Body Syst **52**, 171-187(2012).
- [30] S.Furui, Chaos in Electronic Circuits and Studies of Bifurcation Mechanisms, Proceedings of International Conference of Numerical Analysis and Applied Mathematics 2013(ICNAAM2013), Rhodes, AIP proceedings.